

# Influence of base additives on the reaction-diffusion front of model chemically amplified photoresists

Bryan D. Vogt,<sup>a)</sup> Shuhui Kang, Vivek M. Prabhu,<sup>b)</sup> Ashwin Rao, Eric K. Lin, and Wen-li Wu  
*Polymers Division, National Institute of Standards and Technology, 100 Bureau Dr., Gaithersburg,  
Maryland 20899*

Sushil K. Satija

*Center for Neutron Research, National Institute of Standards and Technology, 100 Bureau Dr.,  
Gaithersburg, Maryland 20899*

Karen Turnquest

*SEMATECH, 2706 Montopolis Dr., Austin, Texas 78741*

(Received 21 July 2006; accepted 6 December 2006; published 11 January 2007)

The effects of amine base quencher on the photoacid catalyzed deprotection reaction-diffusion front in model photoresists were measured by combination of neutron reflectivity and Fourier transform infrared spectroscopy. Modulation in the location of the base with respect to the diffusing photoacid catalyst changes the spatial reaction extent and illuminates the complex role of the base on the shape of the reaction-diffusion front. Despite similar total extents of reaction, a comparison between uniform base and model photodegradable base distributions demonstrates distinct reaction time and base concentration effects on the deprotection profile shape. These differences arise from the modification of the initial deprotection extent due to both the neutralization of the photoacid and the influence of the changing photoresist composition on the reaction-diffusion process. The use of the model photodegradable base results in a sharper front due to these effects. Lastly, aqueous hydroxide development of these latent images demonstrates a limit to the improvement in feature quality obtained from sharpening of the deprotection profile with base additives. © 2007 American Vacuum Society. [DOI: 10.1116/1.2429675]

## I. INTRODUCTION

Pattern formation is commonly accomplished through reaction-diffusion processes by which the diffusivity of the reactants is modulated by the reaction products.<sup>1-3</sup> In microelectronics, an optical image is converted into a chemical latent image via a limited reaction-diffusion process involving a photoacid catalyst.<sup>4,5</sup> As the targeted printed dimensions continue to decrease, this acid diffusion can lead to unacceptable alteration of the feature size and quality (as quantified by line edge roughness).<sup>6</sup> Strategies to control feature quality have historically focused on improving image quality.<sup>7,8</sup> However, recently, Pawloski *et al.* have identified a limiting behavior to the improvement in the final feature quality obtained through improvements in the optical image.<sup>9,10</sup> A key technical challenge for the microelectronics industry is the development of a strategy for further improvements in feature quality beyond this optical limit.<sup>11</sup> The reaction-diffusion process<sup>5,12</sup> that leads to image spreading or blurring<sup>13</sup> has been identified as one factor for feature quality control.<sup>14-16</sup> However, there are several factors that affect the transport properties of the acid catalyst and alter the shape of the deprotection front. In particular, the mobility of the photoacid is significantly reduced upon deprotection of the resist due to changes in the local composition,<sup>17-21</sup>

which can lead to a self-limiting front.<sup>22</sup> Additives to the photoresist can be used to further control the spatial extent of the deprotection front.<sup>23,24</sup>

Base quencher additives have been used commercially in photoresist formulations in attempts to improve performance by limiting diffusion of the photoacid catalyst into unexposed regions.<sup>5,24,25</sup> The influence of these neutralizing species on the reaction-diffusion process is complex.<sup>23</sup> The simplistic view of the quenchers solely acting to neutralize photoacid, thus decreasing the acid concentration, is not always correct.<sup>26</sup> The quencher appears to partially neutralize the photoacid less than stoichiometrically, influence the dissolution either as promoters or inhibitors, and increase the development induction time.<sup>23</sup> The partial neutralization is consistent with the proportional neutralization model of Houle *et al.*, where the added base initially reduces the amount of acid available after photolysis proportional to the base concentration.<sup>17,26,27</sup> Thus, addition of base leads to a reduction in the extent of deprotection, which can be described by a second order reaction in acid and base concentration.<sup>27</sup> Base additives can lead to variation in feature quality, which was attributed to chemical gradients in the resist.<sup>28</sup> These gradients result from the deprotection reaction-diffusion process and can be predicted using the proportional neutralization model.<sup>27</sup> However, direct measurements of the reaction front profile to confirm these predictions are presently lacking.

The role of the base quencher can be systematically examined by placement of the base in a model bilayer, which

<sup>a)</sup>Present address: Department of Chemical Engineering, Arizona State University, Tempe, AZ 85287.

<sup>b)</sup>Author to whom correspondence should be addressed; electronic mail: vprabhu@nist.gov

consists of protected polymer and an acid feeder layer containing a developer soluble polymer and PAG. This bilayer geometry has been used previously to mimic a line edge.<sup>22,27,29–31</sup> Generally, the quencher is not photoactive,<sup>5,32</sup> so base would be located uniformly in both exposed (acid feeder layer of the bilayer) and unexposed (protected layer) regions. This case will be compared to a model photodegradable base geometry in which the base is located only in the protected layer. The mechanism of how the base quencher controls the deprotection spatial extent will be discussed as well as the limitations of profile control on the final aqueous hydroxide developed model line edge.

## II. EXPERIMENT

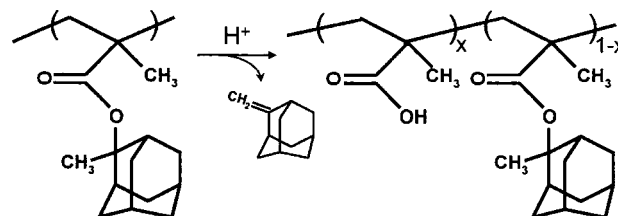
### A. Materials

Poly(methyladamantyl methacrylate) (PMAAdMA, number-average molecular mass ( $M_n$ )=8.8 kg/mol, PDI =1.18) was obtained from Dupont Electronic Materials. PMAAdMA films were spin cast from toluene as PMAAdMA is insoluble in PGMEA. Silicon wafers (76 mm diameter) primed with hexamethyldisilazane were used as substrates. The preparation of the bilayer necessitates the formation of a sharp interface between the two layers after spin coating both layers. The acid feeder layer examined consists of poly(hydroxystyrene) (PHS) (DuPont Electronic Materials,  $M_n$  = 10 000 g/mol) doped with 5% mass fraction of a photoacid generator (PAG), triphenylsulfonium perfluorobutanesulfonate, or nonaflate. The role of base quencher is examined systematically by adding trioctylamine (TOA) selectively to the acid feeder and/or PMAAdMA layers. The adamantyl group on the PMAAdMA is acid cleavable at elevated temperatures. This reaction changes the methyl adamantyl group to a methacrylic acid group and liberates methylene adamantane. Since, methacrylic acid is too weak to catalyze this deprotection reaction,<sup>33</sup> when discussing neutralization of the acid by the base, we are always referring to the photoacid, which is a superacid. The base probably interacts with the methacrylic acid group, but we were unable to separately measure this interaction during the course of the experiments.

Details on the preparation of bilayer films are provided elsewhere.<sup>31</sup> Films are postappily baked at 130 °C to remove residual solvent. The bilayer is exposed to broadband UV radiation (300 mJ/cm<sup>2</sup>) to activate the PAG. A constant post-exposure bake (PEB) temperature of 130 °C is used for the acid-diffusion deprotection reaction. To determine the surface roughness of the bilayers, the acid feeder layer and the deprotected portion of the bottom layer are developed with a 0.26*N* tetramethylammonium hydroxide (TMAH) (Aldrich).

### B. Neutron and x-ray reflectivity

Neutron reflection measurements were performed at the Center for Neutron Research (NCNR) on the NG-7 reflectometer at the National Institute of Standards and Technology (Gaithersburg, MD) in the following configuration: wavelength ( $\lambda$ )=4.768 Å and wavelength spread ( $\Delta\lambda/\lambda$ )=0.025.



SCHEME 1. Acid catalyzed thermally activated deprotection of PMAAdMA. In the presence of the photoacid, the MAAdMA is deprotected to methacrylic acid and methylene adamantane.

The large difference in hydrogen content between PHS and PMAAdMA allows for the bilayer to be resolved with neutron reflectivity (NR). The hydrogen density of the PMAAdMA layer is significantly reduced upon deprotection and loss of methylene adamantane (by-product), thus providing a route for obtaining the deprotection profile through the film thickness. The physical thickness and surface roughness of the films were monitored using x-ray reflectivity (XR).

### C. Fourier transform infrared spectroscopy

The characterization of deprotection reaction (see Scheme 1) and methylene adamantane (MA) residual was made with a Nicolet NEXUS 670 Fourier transform infrared (FTIR) spectrometer equipped with a liquid nitrogen cooled MCT/A detector. Double-side polished with orientation  $\langle 100 \rangle$  and 1–50 Ω cm resistance silicon wafers were used to minimize substrate absorbance. The quantification of deprotection reaction degree is based on the bending vibration mode of CH<sub>3</sub> (1360 cm<sup>-1</sup>) in the protecting MA group of PMAAdMA. The quantification of MA residual level is mainly based on the stretching vibration of H–C(=C) (3065 cm<sup>-1</sup>) in the free MA molecule.<sup>20</sup> The integrated composition of the film determined from FTIR was then used to decompose the  $Q_c^2$  profile obtained from neutron reflectivity to the deprotection level and concentration of methylene adamantane. For comparison purposes, we assume ideal mixing ( $\Delta V_{\text{mix}}=0$ ) to compare FTIR and NR data directly.

### D. Scanned probe microscopy

The developed surface morphology was probed in real space by a Digital Instruments scanned probe microscope (SPM) (Dimension 3100). The experiments were performed in intermittent contact (tapping) mode with silicon cantilevers having a radius of curvature less than 10 nm and tip height of 15–20 μm. Scan size of 5 × 5 μm<sup>2</sup> was used with seven to ten images to calculate the root-mean-square (rms) roughness.

## III. RESULTS

Figure 1 illustrates the change that occurs in the neutron reflectivity profile during the deprotection reaction diffusion for a bilayer containing 0.1% by mass TOA. Prior to deprotection, the bilayer has a sharp interface between the PHS and MAAdMA layer with an interfacial width of less than 25 Å. The amplitude difference between the beating patterns

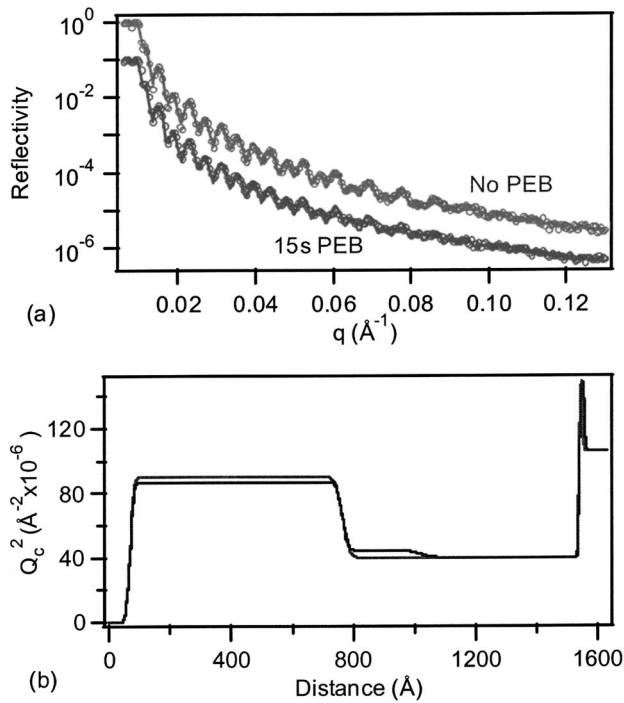


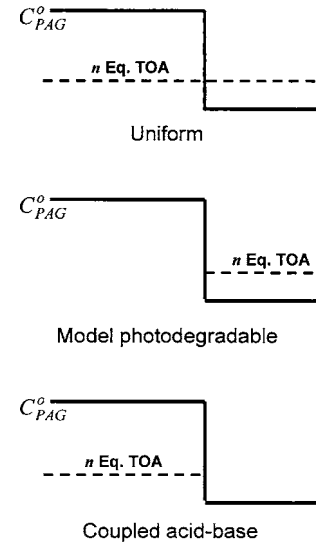
FIG. 1. (a) NR profiles with processing for bilayer containing 0.1 mass % base in MADMA without PEB and after 15 s PEB at 130 °C. The solid lines correspond to the fits of the data as shown in (b).

from the two layers decreases following partial deprotection from a 15 s PEB at 130 °C. This is a result of the decrease in contrast between the PHS and the MADMA layers due to loss of hydrogen content from deprotection and the breath of the deprotection front. The interfacial width between the PHS and MADMA does not change during the PEB. The experimental reflectivity data are fitted using model scattering length density profiles ( $Q_c^2 = 16\pi \sum b_i/v$ ), where the scattering length of each repeat unit is determined by the sum over the atomic scattering lengths  $b_i$  within molar volume ( $v$ ) leading to the absolute scattering length density, an intensive absolute quantity. The reflectivity fits are obtained using the Parratt formalism,<sup>34</sup> where successive layers of constant  $Q_c^2$  with error function interfacial width profiles define the real space depth profile. The total deprotection in the film is determined with FTIR and used to confirm the validity of the NR fits. The general self-consistent methodology to determine the deprotection and residual MA content from NR and FTIR has been reported in detail previously.<sup>22</sup> The general concept is to decompose the  $Q_c^2$  profile in terms of the volume fraction profiles ( $\phi_i$ ) of the individual components with scattering length density ( $Q_{c,i}^2$ ):

$$Q_{c,\text{film}}^2(z) = \phi_{\text{MA}}(z)Q_{c,\text{MA}}^2 + \phi_{\text{MAA}}(z)Q_{c,\text{MAA}}^2 + \phi_{\text{MAdMA}}(z)Q_{c,\text{MAdMA}}^2,$$

$$\phi_{\text{MAdMA}}(z) = 1 - \phi_{\text{MA}}(z) - \phi_{\text{MAA}}(z).$$

FTIR quantifies the integrated amounts of MA, MAA, and MAdMA within the films and these quantities are compared to the integrated fits of  $\phi_{\text{MA}}$  and  $\phi_{\text{MAA}}$  from the NR. If these



SCHEME 2. Depiction of the three different base distributions examined.

values do not agree within 3%, the scattering length density of the deprotected region is changed slightly from the previous fit and while the width and thickness of the deprotection region are allowed to vary during a least squares fit of the NR data. This procedure is repeated until the difference between NR and FTIR is less than 3% for all components. The data are presented along with the standard uncertainty ( $\pm$ ) involved in the measurement based on one standard deviation.

The best fits of the reflectivity profiles from this procedure are shown by the solid lines in Fig. 1(a) with the corresponding  $Q_c^2$  profile in Fig. 1(b). The scattering length of the initial bilayer profile begins in air at zero, then increases to the PHS layer and decreases to the PMAdMA layer. The substrate is then encountered with scattering length densities corresponding to the oxide layer ( $\approx 25$  Å thick) and silicon. After PEB, the  $Q_c^2$  of the MADMA layer near the PHS increases due to the loss of hydrogen content from acid catalyzed deprotection and subsequent partial volatilization of methylene adamantane (MA). This  $Q_c^2$  profile is then converted to the deprotection and MA concentration profiles with use of the FTIR data.

The influence of a base quencher additive, trioctylamine, on the deprotection front profile has been examined systematically, considering both the location of the TOA as well as concentration, as illustrated in scheme 2. In all cases, as the base concentration is increased the total deprotection extent decreases as measured by FTIR. However, the spatial extent is measured using neutron reflectivity. The first case examined is for the homogeneous distribution of base; this is analogous to typical resist formulations. As shown in Fig. 2, addition of TOA to the bilayer significantly alters the deprotection profile. The MADMA nearest the acid feeder layer is no longer fully deprotected with the addition of TOA and the maximum deprotection decreases with increasing base concentration. Additionally, the penetration depth of the deprotection front is decreased, while the width of the front is

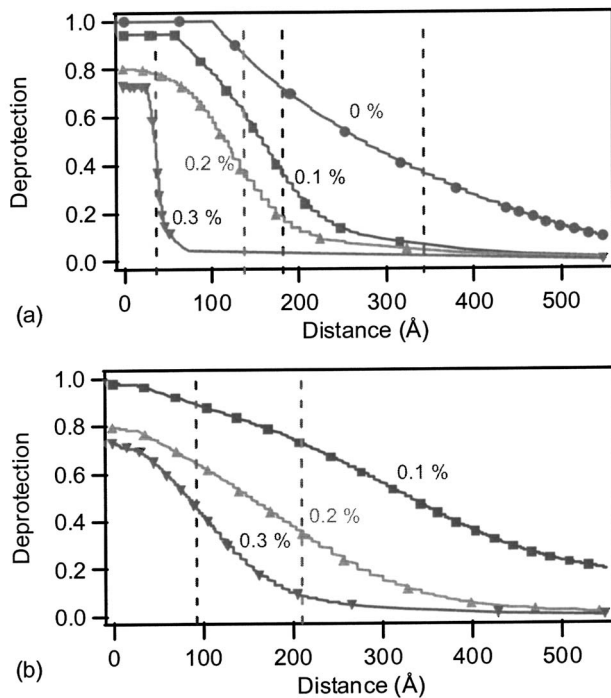


FIG. 2. Deprotection profiles with different base concentrations (●) 0%, (■) 0.1%, (▲) 0.2%, and (▼) 0.3% by mass with TOA uniformly distributed in the bilayer with PEB at 130 °C for (a) 15 s and (b) 60 s. The vertical dashed lines indicate the thickness to which the film dissolves when developed for 60 s in 0.26N TMAH.

sharpened with added TOA. As the PEB time is increased and further reaction diffusion is allowed to occur [Fig. 2(b)], the deprotection level near the acid feeder interface remains nearly constant, while the interface between protected and deprotected MAdMA broadens.

The use of photodegradable bases has been proposed to enhance resist sensitivity and potentially limit line edge roughness (LER). To identify the difference between uniform base and a model photodegradable base on the photoacid reaction-diffusion process, TOA was added only to the MAdMA receiving layer as illustrated in Scheme 2. This strategy was used due to fix the base chemistry while examining the role of the base, because basicity, base size, and hydrophilicity also lead to complex changes in photoresist imaging.<sup>35</sup> In this geometry, the TOA behaves similarly to a photodegradable base, hence this is referred to as a model photobase case (Scheme 2).

An increased TOA concentration in the photobase case decreases the propagation depth of the reaction front and yields a sharper interface between protected and deprotected MAdMA, as shown in Fig. 3. One important difference between this case and the uniform base case is that the deprotection near the acid feeder interface is not dependent upon the TOA concentration. Increasing the diffusion potential of the photoacid through increased PEB time increases the breath of the reaction front, but for concentrations greater than 0.2%, the interface is much sharper for this case of the model photobase than the uniform base.

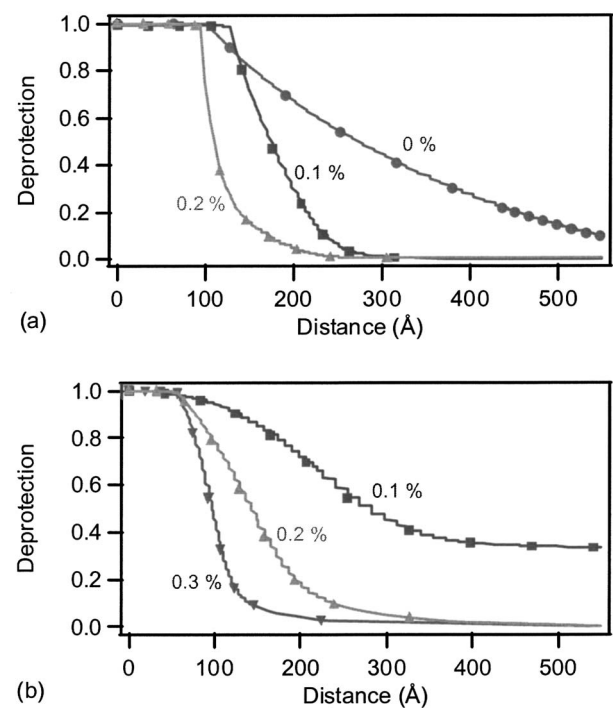


FIG. 3. Deprotection profile with different base concentrations (●) 0%, (■) 0.1%, (▲) 0.2%, and (▼) 0.3% by mass with TOA only in the PMAAdMA layer with PEB at 130 °C for (a) 15 s and (b) 60 s.

To test the role of the base that is in the acid feeder layer, one additional case was examined where the TOA is added only to the acid feeder (Scheme 2). This case is termed coupled acid-base diffusion, as the detection of any influence of the base requires diffusion into the MAdMA layer and subsequent deprotection. The reaction-diffusion fronts obtained from this geometry are illustrated in Fig. 4. These profiles are more similar to the base-free reaction front than those containing base in the receiving layer (Figs. 2 and 3). As the TOA concentration is increased for the coupled acid-base diffusion, the deprotection near the acid feeder layer/MAdMA interface decreases. This case also leads to a very broad deprotection front.

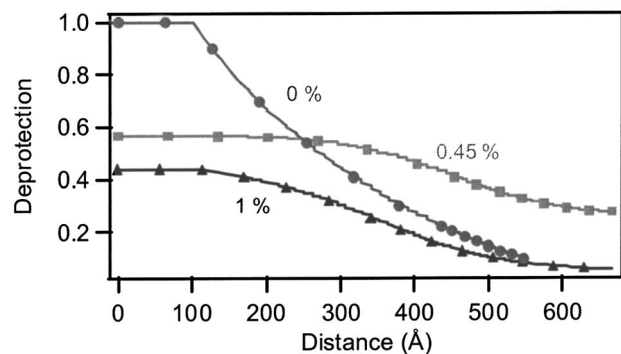


FIG. 4. Deprotection profile with different base concentrations (●) 0%, (■) 0.45%, and (▲) 1%, by mass with TOA only in the acid feeder layer with PEB at 130 °C for 15 s.

## IV. DISCUSSION

### A. Effect of base on latent image

The role of the base quenchers in lithographic patterning is complex and multifaceted, leading to influences on not only the deprotection reaction but also dissolution.<sup>26</sup> This work is focused on determining the influence of the base quenchers on the deprotection profile at the line edge of a latent image through systematic variation of the base quencher concentration and location. One of the simplest approaches is to consider that addition of base simply removes acid from the deprotecting region, where the base neutralizes the acid significantly quicker than the deprotection reaction can occur. This approach is termed proportional neutralization as the photoacid available is reduced proportionally to the amount of base added.<sup>17,26</sup> Another mechanism is competitive neutralization where the acid-base neutralization occurs in competition with the deprotection reaction.<sup>17,26</sup> The experimental data presented here unfortunately cannot distinguish between these models, since the deprotected profiles are measured, not the photoacid distribution after reaction diffusion. For example considering Fig. 2, the deprotection profile broadens as the PEB time is increased from 15 to 60 s for every concentration of base examined. There are two potential sources: additional acid diffuses from the feeder layer to the deprotection front or acid is present beyond the front and is available to catalyze deprotection. The former source is more in line with proportional neutralization, while the latter is more reminiscent of competitive neutralization. Since the acid concentration is not directly measured, but inferred from the deprotection profile, it is not possible to determine the neutralization mechanism. However, these FTIR and NR measurements provide unambiguous answers to the role of base quenchers in defining the deprotection path of the photoacid and are important to development of accurate models of base quenchers for photoresist deprotection.

#### 1. Uniform base

Base quencher additives are common to photoresist formulations; however, the quencher loading and effects are understood primarily via simulation approaches combined with lithographic verification. We have described a uniform base case that mimics this scenario. These concentrations, shown in Fig. 2 (0.1%, 0.2%, and 0.3% mass fractions of TOA), correspond to PAG to base molar ratios of 31:1, 15:1, and 10:1, respectively, and are relevant loadings in photoresist formulations. The addition of base decreases the maximum level of deprotection at the interface with the acid feeder layer; this result is consistent with a decrease in the acid concentration diffusing into the PMAAdMA, either from proportional or competitive neutralization. Additionally, the propagation depth of the deprotection front is decreased and the interface between deprotected and fully protected polymers is sharpened with increasing base concentration. This observation is consistent with the statistical neutralization of the diffusing photoacid. The photoacid diffusion into the

PMAAdMA would result in an error function acid profile, neglecting any instantaneous reactions (deprotection or neutralization). Thus at the leading edge of the photoacid front, neutralization of the acid will be favored due to the low acid concentration relative to the base. The sharp exponential increase in photoacid concentration closer to the acid feeder layer soon overwhelms the base. The resultant photoacid profile after partial neutralization by base should be considerably sharper than the profile without base. This sharp acid profile is primarily responsible for the sharpening of the deprotection front as the TOA concentration is increased. Since the broad leading edge of the photoacid concentration is eliminated, a more uniform deprotection level is initially developed. This deprotection level can retard additional diffusion of the photoacid<sup>21,22</sup> and limit both propagation and broadening of the deprotection front. However, as reaction-diffusion (PEB) time is increased, this front broadens significantly. Previously for a reaction front without base quencher using perfluoro-octanesulfonate as the photoacid counterion, increasing PEB did not significantly broaden the main front, but rather increased the background deprotection.<sup>22</sup> This difference in behavior is an effect of the base additive, where the lower acid concentration leads to lower deprotection extents and hence faster subsequent acid diffusion through this region. Changes in the deprotection path can result in unforeseen effects due to this feedback mechanism due to changes in the acid diffusion from a changing composition induced by the reaction-diffusion process.

#### 2. Model photodegradable base

Additional details on the role of base on the formation of the deprotection front can be elucidated through modulation of the base location, either only in the acid feeder or only in the receiving PMAAdMA layer. The latter mimics a photodegradable base. Comparison of this case (Fig. 3) and the uniform base distribution (Fig. 2) illustrates that placement of the base can influence the deprotection profile. However, from a simplified view, it might be expected that at longer times the profiles would be identical between cases. For example, considering the 0.2% mass fraction TOA case at 60 s, a significantly sharper deprotection front is formed by use of the model photobase. One could hypothesize that at this long time, the initial state would not matter since the acid as it was diffusing through the PMAAdMA has seen the same local base concentration. Clearly, the initial state matters. This result is due to the coupled deprotection extent dependence on the photoacid diffusivity, whereby increased deprotection leads to a decrease in diffusivity. Thus, the initial deprotection profile must influence the propagation of the deprotection front at longer PEB times. For both cases, increasing the TOA concentration sharpens the deprotection front, but the model photobase results in the sharper of the two interfaces. One additional difference in the deprotection profiles is the level of deprotection present at the initial line edge. For the case of uniform base, the deprotection at the interface decreases with addition of TOA, while nearly complete deprotection is observed for all concentrations examined when

TOA is only added to the PMAAdMA layer. We suspect that this behavior is due to the availability of photoacid in the feeder layer; for the former case, photoacid can be neutralized prior to diffusion into the PMAAdMA, while this option does not exist for the latter. The higher deprotection at the initial line edge acts to limit further propagation of the photoacid into the film, which leads to the sharper profile.

One additional consideration for this case is the diffusion of the base into the exposed region due to the steep concentration gradient. The concentration gradient driven mobility of the base was not an issue for the uniform base case described previously, but must be considered for the model photodegradable base distribution. The complete deprotection near the initial line edge implies that the photoacid catalytic activity is not significantly influenced by the counterdiffusion of the base. This observation is consistent with the base remaining stationary during the time scales of the reaction diffusion of the photoacid. Therefore, base diffusion, in this case, may have a minor role in defining the deprotection profile due to a combination of a smaller concentration gradient and a larger molecular size (low diffusivity) in comparison with the photoacid. This result is consistent with kinetic modeling and experiment in which base diffusion in the competitive neutralization is not needed explicitly,<sup>26</sup> once the coupled effect of changing resist chemistry and influence on acid diffusion has been taken into account. However, in the case of a much larger photoacid and high base concentrations, the counterdiffusion of the base molecule must be considered because a gradient in base concentration is present, but this situation is rarely encountered in most relevant photoresist formulations.

### 3. Coupled acid-base diffusion

The final perturbation of the TOA location is where base is only present in the acid feeder layer. Although this case is not pertinent to actual lithographic imaging, it does provide another approach to test our hypothesis developed in the previous two sections as to the role of the base quencher in defining the reaction-diffusion front profile. In this coupled acid-base diffusion case, addition of base broadens the deprotection profile (Fig. 4) for a given reaction (PEB) time unlike the sharpening observed in the previous two cases (Figs. 2 and 3). The propagation distance of the deprotection front exhibits a maximum with addition of TOA to the acid feeder. The source of this counterintuitive behavior is again the decrease in photoacid diffusivity upon deprotection of the PMAAdMA. The base in the top feeder layer acts to partially neutralize the photoacid and decreases the concentration available to diffuse into the PMAAdMA. This change in photoacid concentration decreases the initial deprotection near the acid feeder layer in comparison with the base free case, allowing for further diffusion of the photoacid. The breath of the deprotection front with the addition of either 0.45% or 1% mass fractions TOA in the acid feeder is much greater than obtained without base additives. These measurements illustrate the complex nature of the reaction-diffusion front even in model photoresist systems.

The influences of base on the deprotection are consistent between the three cases examined; one could argue that the uniform base distribution case is simply a composite of the two specialized cases. The deprotection level near the acid feeder layer is decreased through neutralization of the photoacid prior to diffusion into the PMAAdMA. The front is sharpened through neutralization of the leading edge of the reaction-diffusion front. Note that the reaction front is slightly broader for the case of uniform base distribution—consistent with the broadening of the deprotection front found for the addition of TOA to only the acid feeder layer. Unfortunately, a more quantitative description of the base influence is not possible presently. The measurements reported here are for the resultant deprotection profiles, which are related to the local distribution of photoacid and base. However, the exact photoacid and base concentration profiles are not known. Improved methodologies to measure the base diffusion at the very low concentrations present in these photoresist formulations are necessary to further advance models to describe these reaction-diffusion fronts. Partitioning of the base between protected and deprotected regions (as well as the acid feeder) may also be a factor in the local deprotection shape, which due to the feedback mechanism of the reaction-diffusion process will alter the deprotection front profile. However, the low concentration of base in these systems does not allow for direct measurement of the base distribution in the films. This partitioning of base was interpreted to influence LER in photolithographic features.<sup>35</sup>

### B. Development of the bilayers

The latent-image profile characteristics are correlated to the image quality after development as shown by lithographic exposure aerial image quality<sup>8</sup> and image-fading techniques.<sup>9,36</sup> The LER and relationship to the optical image quality can be quantified using the image-log slope (ILS).<sup>36</sup> As the ILS increases an improvement in LER results due to the sharper latent image. However, a plateau effect<sup>36</sup> in LER was observed beyond  $ILS = 15 \mu\text{m}^{-1}$ . In comparison with the present model experiments, an ILS of order  $600\text{--}1000 \mu\text{m}^{-1}$  is calculated, since interfacial width varies between 2 and 3 nm.<sup>37</sup> Hence, this profile is degraded via photoacid reaction diffusion permitting a focused discussion on the materials process effects, rather than optical image quality. This approach distinguishes the current model experiments from the previous lithographic studies. We now discuss the effect of base on the relationship between the profile shape quantified as the latent-image log-slope and the SPM surface roughness.

The changes in the propagation depth of the reaction front with base concentration allow improved control of critical dimensions. Development of the bilayers with 0.26N TMAH dissolves the top PHS acid feeder as well as some of the partially deprotected PMAAdMA. The solubility switch for this material is approximately 40%–45% deprotection<sup>20,22</sup>—thus chains with greater than this fraction deprotection are soluble in the developer and are removed, while chains with a lesser degree of deprotection are in-

TABLE I. Surface roughness obtained from SPM for developed bilayers (for 15 s PEB).

Bilayer type	Base concentration (% by mass)	Surface roughness (nm)
As-spun, postdeveloped films		0.3±0.1
No base	0	3.8±1.3
Coupled acid-base	0.45	2.0±0.4
Coupled acid-base	1.0	2.6±0.4
Uniform	0.1	1.4±0.3
Uniform	0.2	1.8±0.1
Uniform	0.3	1.5±0.1
Uniform	0.45	1.4±0.1
Model photobase	0.1	1.5±0.1
Model photobase	0.2	1.8±0.1
Model photobase	0.3	1.5±0.1
Model photobase	0.45	1.2±0.2

soluble. Based upon the geometry of the bilayer, the developed surface is analogous to the edge of a developed line. The surface roughness for the developed bilayers (PEB = 15 s at 130 °C) is shown in Table I. The surface roughness does not change dramatically for either the uniform or model photobase cases. However, these are less than the roughness found for the bilayer without base or when using the coupled acid-base bilayer.

Considering the LER dependence on initial image quality, it is surprising that the shape of the deprotection profile does not significantly influence LER. However, the initial ILS is extremely high, thus the subsequent reaction diffusion might be insufficient to degrade the image quality to the point where an increase in LER is observed. Because the real space deprotection profiles are available, we can define a metric analogous to ILS, which defines the optical image quality, for the deprotection profile shape; the latent-image slope. The latent-image slope is defined as the slope in the deprotection profile between deprotection extents of 0.35 and 0.5. Because the exposure dose remains constant in these experiments, the latent-image slope is truly analogous to ILS. Figure 5 illustrates the influence of latent-image slope on the developed roughness of the bilayer in terms of the rms roughness. At low latent-image slope ( $<20 \mu\text{m}^{-1}$ ), there is an increase in the roughness of the developed bilayers similar to the increase in LER observed lithographically for  $\text{ILS} < 15 \mu\text{m}^{-1}$ .<sup>28,36</sup> At larger latent-image slope, a plateau in the roughness is found with a limiting value of approximately 1.5 nm.

Thus, the limit in surface roughness is not solely due to the blur from the reaction-diffusion process. This result means that sharpening the deprotection front will only improve LER to its limiting value. However, because the model photobase results in a sharper deprotection profile than obtained for the uniform base at identical processing conditions, a photodegradable base should allow for high quality features to be printed at lower ILS than can be used for a typical base in lithographic processing. The latent-image

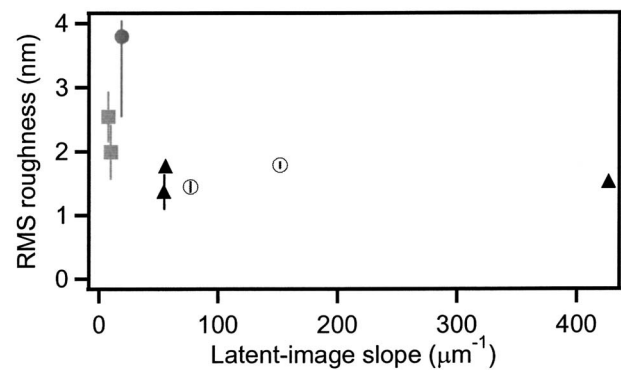


FIG. 5. rms roughness of developed bilayers as determined by SPM for different base locations: (●) no base, (■) coupled acid-base, (▲) uniform base, (○) model photobase. As the latent-image slope increases, there is an improvement in the rms roughness to a finite limit of approximately 1.5 nm.

slope data suggest that strategies focused on another processing step such as development may be needed for any additional improvement in surface roughness beyond those that control the deprotection profile shape.

## V. CONCLUSIONS

The influence of a model base quencher, trioctylamine, on the deprotection front profile at a model line edge (bilayer) was determined through systematic variation of the base location in three cases: uniform base, a model photodegradable base, and coupled acid-base diffusion. The deprotection profiles from these cases were determined using a combination of neutron reflectivity and FTIR. Base in the acid feeder layer (“exposed” regions) leads to a decrease in the level of deprotection near the initial line edge and broadens the deprotection front profile. Conversely, base in the MADMA layer (“unexposed” regions) leads to a sharper deprotection front profile and decreases the propagation of the reaction front. A sharper deprotection front leads to an improvement in the developed surface roughness of the bilayers to a limit of 1.5 nm. The model photodegradable base provides a sharper deprotection front than that obtained for the uniform base at identical processing conditions. Thus, it is probable that use of photodegradable bases would improve the lithographic capabilities of photoresists, based on the latent-image quality improvement.

## ACKNOWLEDGMENTS

This work was supported by SEMATECH under Agreement No. 309841 OF. The authors acknowledge Jim Sounik and Michael Sheehan at DuPont Electronic Polymers for providing the polymers used in this study. This is an official contribution of the National Institute of Standards and Technology, not subject to copyright in the United States.

<sup>1</sup>A. M. Turing, Philos. Trans. R. Soc. London, Ser. B **237**, 37 (1952).

<sup>2</sup>Q. Ouyang and H. L. Swinney, Nature (London) **352**, 610 (1991).

<sup>3</sup>E. O. Budrene and H. C. Berg, Nature (London) **349**, 630 (1991).

<sup>4</sup>H. Ito, IBM J. Res. Dev. **44**, 119 (2000).

<sup>5</sup>H. Ito, Adv. Polym. Sci. **172**, 37 (2005).

- <sup>6</sup>T. Yoshimura, Y. Nakayama, and S. Okazaki, *J. Vac. Sci. Technol. B* **10**, 2615 (1992).
- <sup>7</sup>H. J. Levinson and W. H. Arnold, *J. Vac. Sci. Technol. B* **5**, 293 (1987).
- <sup>8</sup>W. Hinsberg, F. A. Houle, J. Hoffnagle, M. Sanchez, G. Wallraff, M. Morrison, and S. Frank, *J. Vac. Sci. Technol. B* **16**, 3689 (1998).
- <sup>9</sup>A. R. Pawloski, A. Acheta, H. J. Levinson, T. B. Michaelson, A. Jamieson, Y. Nishimura, and C. G. Willson, *J. Microlithogr., Microfabr., Microsyst.* **5**, 023001 (2006).
- <sup>10</sup>A. Pawloski, A. Acheta, I. Lalovic, B. LaFontaine, and H. Levinson, *Proc. SPIE* **5376**, 414 (2004).
- <sup>11</sup>International Technology Roadmap for Semiconductors 2005 Edition Lithography, <http://www.itrs.net/Links/2005ITRS/Litho2005.pdf>, 2005.
- <sup>12</sup>G. M. Wallraff *et al.*, *Proc. SPIE* **4690**, 160 (2002).
- <sup>13</sup>F. A. Houle, W. D. Hinsberg, M. I. Sanchez, and J. A. Hoffnagle, *J. Vac. Sci. Technol. B* **20**, 924 (2002).
- <sup>14</sup>J. H. Kim, Y. H. Kim, S. M. Chon, T. Nagai, M. Noda, Y. Yamaguchi, Y. Makita, and H. Nemoto, *J. Photopolym. Sci. Technol.* **17**, 379 (2004).
- <sup>15</sup>G. M. Schmid, M. D. Stewart, V. K. Singh, and C. G. Willson, *J. Vac. Sci. Technol. B* **20**, 185 (2002).
- <sup>16</sup>M. D. Stewart, H. V. Tran, G. M. Schmid, T. B. Stachowiak, D. J. Becker, and C. G. Willson, *J. Vac. Sci. Technol. B* **20**, 2946 (2002).
- <sup>17</sup>W. Hinsberg *et al.*, *Proc. SPIE* **3999**, 148 (2000).
- <sup>18</sup>F. A. Houle, W. D. Hinsberg, M. Morrison, M. I. Sanchez, G. Wallraff, C. Larson, and J. Hoffnagle, *J. Vac. Sci. Technol. B* **18**, 1874 (2000).
- <sup>19</sup>S. Kang, V. M. Prabhu, B. D. Vogt, E. K. Lin, W. L. Wu, and K. Turnquest, *Proc. SPIE* **6153**, 61533N (2006).
- <sup>20</sup>S. Kang, V. M. Prabhu, B. D. Vogt, E. K. Lin, W.-I. Wu, and K. Turnquest, *Polymer* **47**, 6293 (2006).
- <sup>21</sup>S. V. Postnikov *et al.*, *J. Vac. Sci. Technol. B* **17**, 3335 (1999).
- <sup>22</sup>B. D. Vogt, S. Kang, V. M. Prabhu, E. K. Lin, S. K. Satija, K. Turnquest, and W. L. Wu, *Macromolecules* **39**, 8311 (2006).
- <sup>23</sup>A. R. Pawloski, Christian, and P. F. Nealey, *Chem. Mater.* **14**, 4192 (2002).
- <sup>24</sup>F. Houlihan, D. Person, I. Rushkin, O. Dimov, E. Reichmanis, and O. Nalamasu, *J. Photopolym. Sci. Technol.* **14**, 373 (2001).
- <sup>25</sup>F. Houlihan, D. Person, O. Nalamasu, I. Rushkin, O. Dimov, and E. Reichmanis, *Proc. SPIE* **4345**, 67 (2001).
- <sup>26</sup>F. A. Houle, W. D. Hinsberg, and M. I. Sanchez, *J. Vac. Sci. Technol. B* **22**, 747 (2004).
- <sup>27</sup>W. D. Hinsberg, F. A. Houle, M. I. Sanchez, and G. M. Wallraff, *IBM J. Res. Dev.* **45**, 667 (2001).
- <sup>28</sup>T. B. Michaelson, A. R. Pawloski, A. Acheta, Y. Nishimura, and C. G. Willson, *Proc. SPIE* **5753**, 368 (2005).
- <sup>29</sup>F. A. Houle, W. D. Hinsberg, and M. I. Sanchez, *Macromolecules* **35**, 8591 (2002).
- <sup>30</sup>E. K. Lin *et al.*, *Science* **297**, 372 (2002).
- <sup>31</sup>R. L. Jones, V. M. Prabhu, D. L. Goldfarb, E. K. Lin, C. L. Soles, J. L. Lenhart, W. L. Wu, and M. Angelopoulos, *Polymers for Microelectronics and Nanoelectronics ACS Symposium Series* **874**, 86 (2004).
- <sup>32</sup>S. Funato *et al.*, *Proc. SPIE* **2724**, 186 (1996).
- <sup>33</sup>P. J. Paniez, S. Gally, B. P. Mortini, C. Rosilio, P.-O. Sassoulas, R. R. Dammel, M. Padmanaban, A. Klauk-Jacobs, and J. E. Oberlander, *Proc. SPIE* **3678**, 1352 (1999).
- <sup>34</sup>L. G. Parratt, *Phys. Rev.* **95**, 359 (1954).
- <sup>35</sup>*Proc. SPIE* **6153**, 615317 (2006).
- <sup>36</sup>A. Pawloski, A. Acheta, I. Lalovic, B. La Fontaine, and H. Levinson, *Proc. SPIE* **5376**, 414 (2004).
- <sup>37</sup>The ILS was calculated by evaluating the slope at the dose profile midpoint;  $ILS = I(z)^{-1} DI(z)/Dz$ .